Neuron
Article

Distinct Cortical Circuit Mechanisms for Complex Forelimb Movement and Motor Map Topography

Thomas C. Harrison,[1,2] Oliver G.S. Ayling,[1,2] and Timothy H. Murphy[1,2,*]
[1]Department of Psychiatry
[2]Brain Research Centre
University of British Columbia, Vancouver, BC V6T 1Z3, Canada
*Correspondence: thmurphy@mail.ubc.ca
DOI 10.1016/j.neuron.2012.02.028

SUMMARY

Cortical motor maps are the basis of voluntary movement, but they have proven difficult to understand in the context of their underlying neuronal circuits. We applied light-based motor mapping of Channelrhodopsin-2 mice to reveal a functional subdivision of the forelimb motor cortex based on the direction of movement evoked by brief (10 ms) pulses. Prolonged trains of electrical or optogenetic stimulation (100–500 ms) targeted to anterior or posterior subregions of motor cortex evoked reproducible complex movements of the forelimb to distinct positions in space. Blocking excitatory cortical synaptic transmission did not abolish basic motor map topography, but the site-specific expression of complex movements was lost. Our data suggest that the topography of movement maps arises from their segregated output projections, whereas complex movements evoked by prolonged stimulation require intracortical synaptic transmission.

INTRODUCTION

The motor cortex has long been known to play a central role in the generation of movement (Fritsch and Hitzig, 1870), but fundamental questions remain to be answered about the functional organization of its subregions and their neuronal circuits. Results from electrical brain stimulation have traditionally been interpreted with an emphasis on somatotopy (Penfield and Boldrey, 1937; Asanuma and Rosén, 1972), but the utility of this principle has diminished with the discovery of multiple representations of the body (Neafsey and Sievert, 1982; Luppino et al., 1991; Schieber, 2001). A more nuanced view has since developed, with recordings made during voluntary movements in monkeys demonstrating that neurons in motor cortex encode information related to the force (Evarts, 1968), direction (Georgopoulos et al., 1986), and speed of movements (Moran and Schwartz, 1999; Churchland et al., 2006). The activity of cortical neurons also reflects both preparation for movement (Sanes and Donoghue, 1993; Paz et al., 2003) and the interpretation of actions performed by others (Gallese et al., 1996; Hari et al., 1998). Recently, experimentation with prolonged trains of stimulation has suggested that the brain's multiple motor representations may be organized according to classes of behavior (Graziano et al., 2002; Stepniewska et al., 2005; Ramanathan et al., 2006).

Despite the detailed knowledge gleaned from these efforts, our understanding of the macroscopic organization of motor cortex remains incomplete. Much of our understanding about the motor cortex comes from experiments in which stimulation or recording is performed at a few cortical points. Technical limitations have traditionally made it difficult to probe the cortical circuitry underlying motor representations in a uniform, quantitative manner. Recently, we and others have developed a novel method for rapid automated motor mapping based on light activation of Channelrhodopsin-2 (ChR2) that has facilitated experiments which were previously impossible (Ayling et al., 2009; Hira et al., 2009; Komiyama et al., 2010). This technique has the advantage of objectively and reproducibly sampling the movements evoked by stimulation at hundreds of cortical locations in mere minutes. Here, we apply light-based motor mapping to investigate the functional subdivisions of the motor cortex and their dependence on intracortical activity.

The ability to repeatedly map the motor cortex over timescales ranging from minutes to months has allowed us to appreciate the dynamic nature of movement representations and facilitated the comparison of motor maps generated before and after pharmacological perturbations of the intracortical circuitry. We have exploited the predominant expression of Channelrhodopsin-2 in layer 5B pyramidal neurons of *Thy-1* transgenic mice (Arenkiel et al., 2007; Wang et al., 2007; Yu et al., 2008; Ayling et al., 2009) to target this class of corticofugal cells directly, exposing their contribution to motor cortex topography and identifying a functional subdivision of the mouse forelimb representation based on movement direction. Prolonged trains of light or electrical stimulation revealed that activation of these subregions drives movements to distinct positions in space. To identify mechanisms that could account for the different movement types evoked by stimulation of these cortical subregions, we performed pharmacological manipulations of the intracortical circuitry and targeted anatomical tracing experiments.

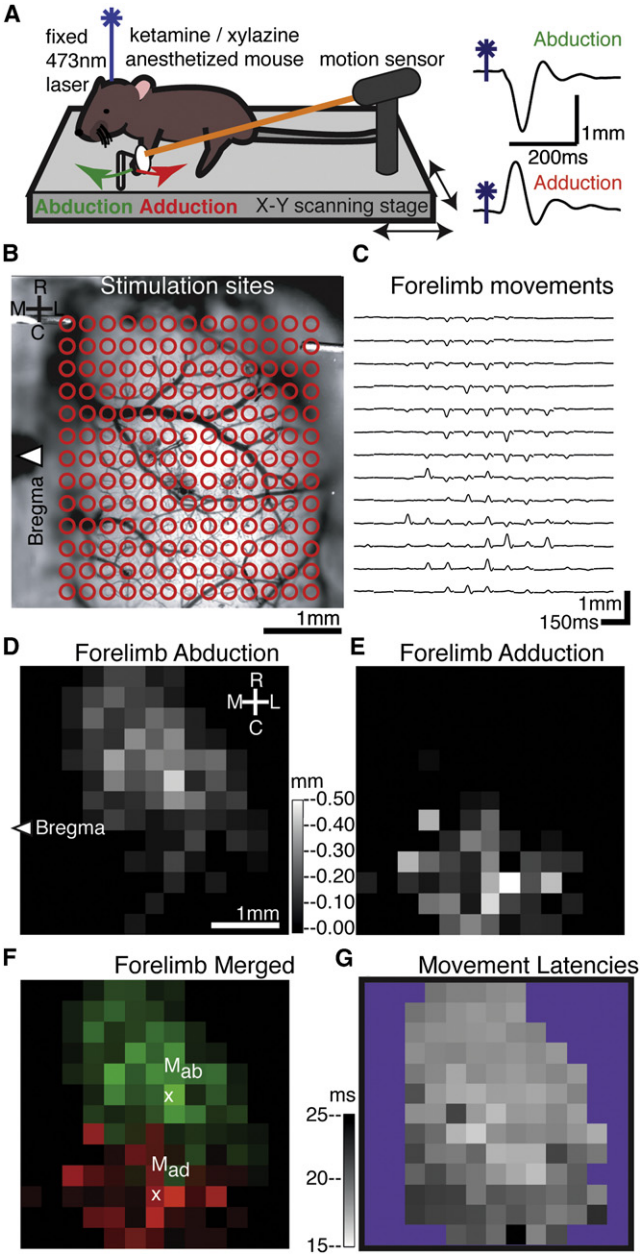

Figure 1. Spatial Heterogeneity of Evoked Movements Revealed by Light-Based Motor Cortex Mapping

(A) Anesthetized, head-fixed mice were placed in the prone position with their contralateral forelimb suspended to allow free forward or backward movement (left). Forelimb movements evoked by optogenetic cortical stimulation were assayed as either abduction or adduction depending on the direction of movement recorded by a noninvasive motion sensor (right). Mapping was relatively noninvasive and could be performed repeatedly in the same animal (see Figure S1).

(B and C) By delivering three repetitions of stimulation to an array of cortical points in random order (B), a map of averaged evoked movements (C) was assembled. Note the heterogeneity of movements in this representative example.

(D and E) The same movements classified by direction and scaled by amplitude to form separate maps of forelimb abduction and adduction.

(F) Merged motor map, with sites from which abduction movements were evoked in green (M_{ab}, center of gravity marked with an x), and adduction sites in red (M_{ad}). Similar maps were generated in animals where expression of ChR2 was mediated by viral transduction (see Figure S2).

(G) Latencies from stimulus onset to movement onset for each of the cortical sites in (F).

All data in this figure are from the same representative animal.

RESULTS

Movement-Based Mapping of Mouse Motor Cortex

We used optogenetic motor mapping to rapidly stimulate hundreds of cortical points in ChR2 transgenic mice (Arenkiel et al., 2007) and assemble maps based on evoked movements of the contralateral forelimb and hindlimb (Figures 1A–1C, see Ayling et al., 2009 for methodological details). In these experiments, anesthetized mice were head-fixed in the prone position with their contralateral limbs suspended. In this posture, the limbs were able to move freely along the axis of measurement of a laser range finder. The resultant movement maps were centered at positions consistent with those obtained by EMG recording or visual observation (forelimb: 2.2 ± 0.1 mm lateral, 0.05 ± 0.09 mm anterior of bregma; hindlimb: 2.0 ± 0.11 mm lateral, 0.21 ± 0.1 mm posterior of bregma, n = 14 mice, all values ± SEM) (Pronichev and Lenkov, 1998; Ayling et al., 2009; Hira et al., 2009; Tennant et al., 2011). Composite maps based on the average of three repetitions were highly reproducible, with a shift in center position of 0.19 ± 0.02 mm (n = 12 mice) between mapping trials (~30 min per composite map). In a separate group of animals implanted with cranial windows, maps remained stable for months (Figure S1 available online). Movement maps could also be generated in animals where ChR2 was expressed in pyramidal neurons of both superficial and deep cortical layers by transduction with adeno-associated virus (Figure S2).

Forelimb Motor Cortex Is Subdivided into Functional Subregions

Consistent with previous results, forelimb movements could be elicited by stimulation (10 ms pulses, 0.5–10 mW or 63–1270 mW/mm^2) of a broad cortical area, up to 2 mm anterior and posterior of bregma (Ayling et al., 2009; Tennant et al., 2011). However, when forelimb movements were examined at stimulation sites across the motor cortex, a diversity of response types became apparent (Figures 1C–1F). Evoked movements were divided into two classes depending on the direction of forelimb movement (abduction or adduction, Figures 1D–1F). Stimulation sites that produced movements containing both abduction and adduction components were considered as regions of overlap between abduction and adduction maps. This analysis revealed a functional subdivision of the motor cortex that was not apparent from EMG-based maps, even when antagonistic muscle pairs were compared (Ayling et al., 2009).

The motor cortex abduction representation (here termed M_{ab}) was not different from the adduction representation in area (M_{ad}) (4.7 ± 0.6 versus 4.9 ± 0.7 mm^2, n = 14 mice), but movements evoked from the center of M_{ab} tended to be smaller than those

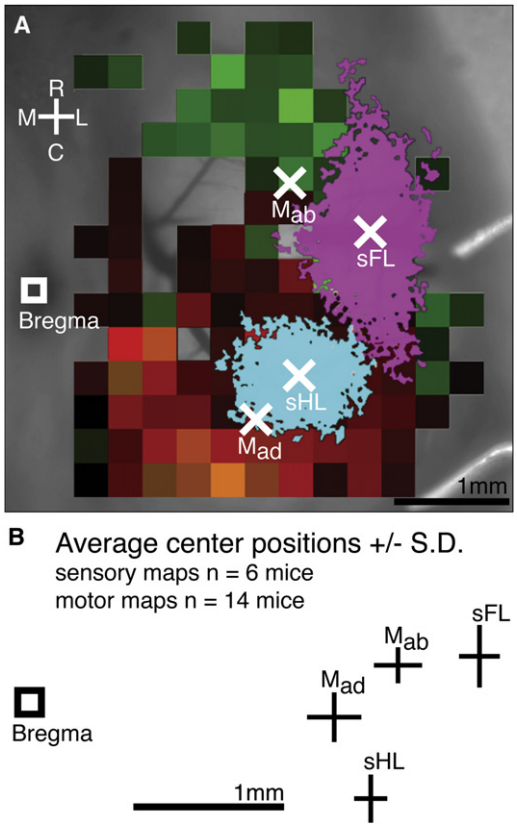

Figure 2. Relative Positions of Motor and Somatosensory Representations

(A) Representative motor maps (M_{ab} in green, M_{ad} in red) thresholded at 0.1 mm of limb displacement and overlaid onto an image of the cortex. Somatosensory representations of the forelimb (sFL, purple) and hindlimb (sHL, cyan) were generated by intrinsic optical signal imaging and thresholded at 0.02% change in reflectance of 635 nm light. White crosses mark the center of gravity for each representation.

(B) Mean positions of the centers of gravity with respect to bregma for each of these representations, with the variability of the coordinates (standard deviation) represented by the lengths of the cross-bars (n = 6 mice for sensory maps and 14 mice for motor maps).

evoked from the center of M_{ad} (0.2 ± 0.02 versus 0.5 ± 0.09 mm, p = 0.036 paired t test, n = 14 mice). M_{ab} movements also began at a shorter latency from the onset of cortical stimulation (19.4 ± 0.9 versus 24.6 ± 1.5 ms, p = 0.002 paired t test, n = 14 mice) (Figure 1G). M_{ab} was typically located anterior and lateral of M_{ad} (Figures 2A and 2B). M_{ab} and M_{ad} were both centered within the boundaries of the caudal forelimb area defined by intracortical electrical microstimulation, but frequently extended into the reported territory of the rostral forelimb area (Tennant et al., 2011). The M_{ad} portion of the forelimb map overlapped with hindlimb motor cortex to a greater extent than M_{ab} (55.9 ± 8.7 versus 43.9 ± 7.5%, n = 14 mice, p < 0.01, paired t test). M_{ad} was also closer than M_{ab} to the centers of the hindlimb somatosensory representation, whereas M_{ab} was closer than M_{ad} to the center of the forelimb somatosensory representation (Figure 2B). M_{ab} and M_{ad} representations were not different in consistency, defined as the percentage of stimulus sites from which movements were evoked in all three repetitions of a composite map (8.3 ± 2.3 versus 10.8 ± 3.0%, n = 12 mice). The centers of gravity of M_{ab} and M_{ad} were separated from each other by an average of 0.6 ± 0.06 mm (p < 0.0001, single sample t test versus hypothetical mean 0, n = 14 mice). When a threshold was applied at 50% of each map's peak amplitude, separation between M_{ab} and M_{ad} increased to 1.2 ± 0.07 mm (n = 14 mice), which is comparable to the distance between the centers of forelimb and hindlimb somatosensory maps (1.2 ± 0.2 mm, n = 7 mice). These observations demonstrate that the mouse forelimb motor cortex can be reproducibly subdivided according to a simple assay of evoked movement direction.

Prolonged Stimulation of Abduction and Adduction Representations Drives Movements to Distinct Positions in Space

It has been proposed that long stimulus trains may be more effective than shorter bursts at producing ethologically relevant movements and identifying cortical movement representations (Graziano et al., 2005). Despite the ability of light-based mapping to rapidly, quantitatively, and uniformly sample the motor output of a large cortical area, the restricted sampling of forelimb displacement in our method limits the information that can be gathered about the movements generated by stimulation of any particular cortical location. To better describe the properties of the M_{ab} and M_{ad} motor subregions, we used a high-speed CCD camera to record forelimb movements evoked by stimulation of sites near the center of each map. In these experiments, the centers of the M_{ab} and M_{ad} maps were defined with the mouse lying prone and the contralateral forelimb suspended parallel to the ground (Figure 3A, left). The anesthetized mice were then moved to a sitting posture, with their heads fixed and their forelimbs hanging free (Figure 3A, center).

With prolonged stimulus trains (500 ms), the forelimb tended to reach a final position within ~300 ms and remain there for the duration of the stimulus. Stimulation of M_{ab} caused the contralateral forelimb to be raised and then brought toward the midline, whereas stimulation of M_{ad} typically produced rhythmic movements lower in space, often coupled with movement of the hindlimb (Figure 3B). These movements were reproduced in anesthetized mice where ChR2 was locally expressed using adeno-associated virus (Figure S2) and in awake, freely moving ChR2 transgenic mice stimulated within M_{ab} and M_{ad} via optical fibers (Figures 3A and 3B, right; Movie S2). In both anesthetized and awake mice, the displacement of the limb from its starting position was significantly greater when M_{ab} was stimulated rather than M_{ad} (Figures 3B and 3C). Although movement trajectories (Figure 3B) and displacements (Figure 3C) were clearly dependent on stimulus site for both awake and anesthetized mice, the speed profiles of M_{ab} and M_{ad} movements were nearly identical (Figure 3D). Movements evoked from each site were remarkably consistent from trial to trial, and the variability that they did exhibit had a temporal structure that depended on the site of stimulation (Figure S3). Increasing stimulus duration generally had little effect on movement map structure, despite changes observed in movement trajectories (Figure S4). Consistent with previous results from electrical

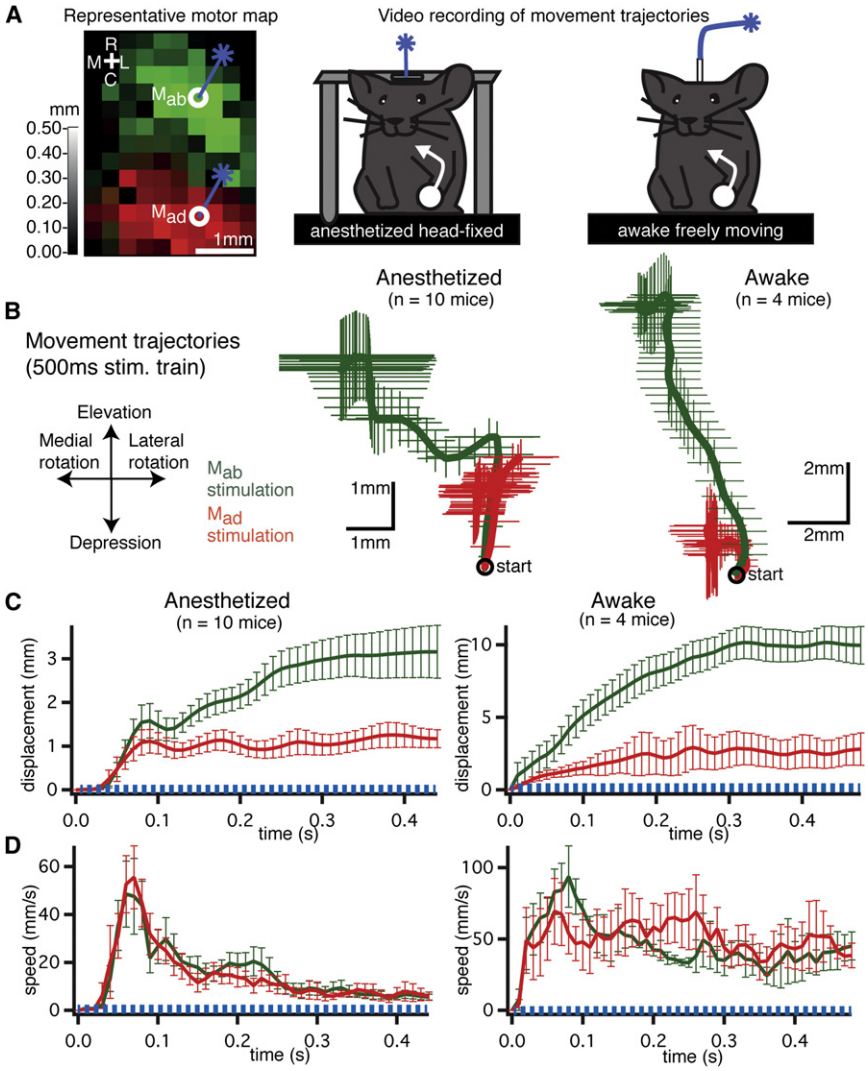

Figure 3. Complex Movements Evoked by Prolonged Stimulation of the Abduction or Adduction Representations

(A) Representative forelimb motor map generated with pulses (10 ms) of 473 nm light (left). After identifying the centers of gravity of the abduction (M_{ab}) and adduction (M_{ad}) representations in anesthetized animals, the center of each representation was stimulated with trains of light stimulation (left) while the resulting movements were captured by high-speed video to reconstruct movement trajectories (center). In separate experiments, M_{ab} and M_{ad} were stimulated alternately via optical fibers in awake, freely moving animals (right).

(B) Mean trajectories of movements evoked in anesthetized (left) and awake (right) animals by stimulation of M_{ab} (green) and M_{ad} (red) marked with error bars (SEM). Movements evoked from a given site are highly reproducible within animals (see Figure S4). Movement trajectories are strongly dependent on stimulus duration, but movement maps are not (see Figure S5).

(C) Mean forelimb displacement for the movements depicted in B. Dashed blue lines above the abscissae denote the period of stimulation. Movements evoked by stimulation of M_{ab} are significantly larger than M_{ad} in anesthetized animals ($F[1,44]_{stim\ site} = 12.36$, $p = 0.0025$, $F[1,44]_{interaction} = 5.638$, $p < 0.0001$, RM-ANOVA, $n = 10$) and in awake animals ($F[1,49]_{stim\ site} = 557.4$, $p < 0.0001$, $F[1,49]_{interaction} = 1.661$, $p = 0.01$ RM-ANOVA, $n = 4$).

(D) Speed profiles for the movements shown in (B). Note that despite differences in movement trajectory, speed profiles are almost identical for both anesthetized and awake animals. Error bars in all graphs are SEM.

stimulation (Ramanathan et al., 2006), modulating optogenetic stimulus intensity did not affect movement trajectories evoked by prolonged stimulation (Figure S5). These experiments complement the mapping study by exposing the distinct types of complex movement that can be evoked from M_{ab} and M_{ad} by prolonged stimulation in both anesthetized and awake mice.

Electrical and Optogenetic Stimulation Evoke Similar Movements

To determine whether these complex movements require selective stimulation of layer 5B neurons, we compared optogenetic stimulation (500 ms train of 5 ms, 5 mW pulses at 100 Hz) with trains of electrical intracortical microstimulation (ICMS) targeted to layer 5 of cortex (500 ms trains of 200 μs, 100 μA pulses at 200 Hz) (Ramanathan et al., 2006). Given the differences between ICMS and optogenetic stimulation, we were surprised to discover that ICMS was able to closely reproduce the complex movements characteristic of transgenic or viral optogenetic stimulation of M_{ab} and M_{ad} (Figure 4A, Figure S2). In addition to their overlapping trajectories, movements evoked by either method had comparable peak displacements, time to peak, and angle from origin at peak displacement (Figure 4B). Interestingly, although movements evoked by ICMS or optogenetic stimulation shared the same end point, ICMS-evoked movements were significantly slower (Figure 4C). These results suggest that the site of stimulation determines the trajectory of the resulting movement (Figure 3), whereas movement speed depends on the mechanism of stimulation (Figure 4).

Specificity of Complex Movements Evoked from Different Cortical Areas Requires Intracortical Synaptic Transmission

After characterizing the movement representations of the mouse motor cortex, we investigated their mechanistic basis. We hypothesized that the distinct movements produced by the M_{ab} and M_{ad} motor cortex subregions could be explained by differences either in their output projections (Rathelot and Strick, 2009; Matyas et al., 2010), or in the pattern of input they receive

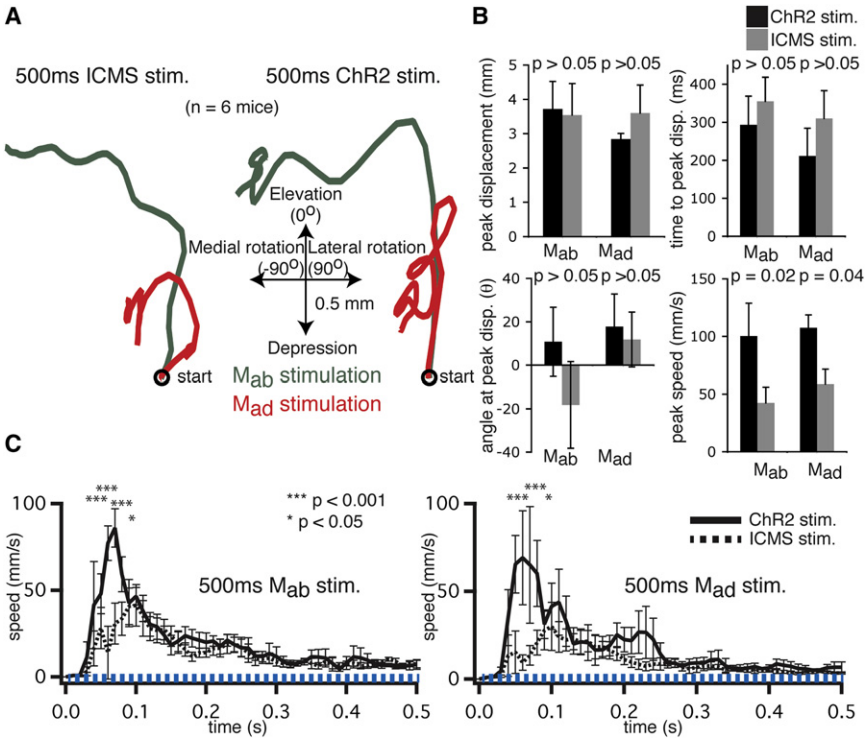

Figure 4. Optogenetic and Electrical Stimulation Evoke Similar Complex Movements

(A) Mean trajectories of movements evoked by 500 ms of electrical (left) or optogenetic stimulation (right) of the M_{ab} (green) and M_{ad} (red) representations in the same animals.

(B) These movements did not differ in peak displacement, time to peak displacement, or angle from origin at peak displacement. Peak movement speed was greater for optogentically evoked M_{ab} and M_{ad} movements (paired t tests).

(C) Speed profiles for the movements depicted in (A). Solid black lines correspond to optogenetically evoked movements, dashed black lines to electrically evoked movements. Dashed blue lines above the abscissae denote the period of stimulation. Despite similar movement trajectories (A), speed profiles were strongly dependent on stimulus type for both M_{ab} (left, $F(1,50)_{stim\ type} = 28.41$, $p < 0.0001$, $F(1,50)_{interaction} = 1.682$, $p = 0.0033$, RM-ANOVA with Bonferroni posttest results indicated by asterisks on graph) and for M_{ad} (right, $F[1,50]_{stim\ type} = 24.68$, $p < 0.0001$, $F[1,50]_{interaction} = 2.798$, $p = 0.0033$). Increasing stimulus intensity had no effect on complex movement trajectories, but did increase map area (see Figure S6).

Error bars in all graphs are SEM.

from recurrent intracortical circuits (Weiler et al., 2008; Anderson et al., 2010; Hooks et al., 2011) or subcortical loops (Hoover and Strick, 1993; Flaherty and Graybiel, 1991; Kelly and Strick, 2003). To test the extent to which cortical synaptic input contributes to the differences between M_{ab} and M_{ad} motor subregions, we compared movement trajectories generated before and after the application of glutamate receptor antagonists (CNQX 4.5 mM and MK-801 0.3 mM) or saline to the cortical surface (Figure 5A). In the control condition M_{ab} and M_{ad} movements had nonoverlapping trajectories that could be distinguished by plotting the angle of the forelimb from the starting position (Figure 5B, left). Disrupting glutamatergic transmission increased the extent to which M_{ab} and M_{ad} trajectories overlapped, biasing both toward medial rotation (Figure 5B, right). Glutamate receptor antagonists also had a site-specific effect on speed profiles, causing a delayed increase in movement speed for M_{ad}, but not M_{ab} (Figure 5C). These results suggest that differences between movements evoked by prolonged stimulation of M_{ab} and M_{ad} may reflect variation in the patterns of glutamatergic synaptic input that these areas receive.

Movement Topography Is Preserved during Blockade of Intracortical Synaptic Transmission

We next examined the effects of pharmacological manipulations on the structure of motor maps evoked by brief (10 ms) pulses of light (Figures 6A and 6B). We had initially hypothesized that blocking cortical glutamatergic transmission would eliminate the contribution of facilitatory cortico-cortical projections from regions lacking direct motor output, causing a reduction in map area. Surprisingly, we found that M_{ab} and M_{ad} maps tended to increase in amplitude (Figure 6B) and expand in area (Figure 6C) after application of glutamate receptor antagonists, compared with no change after application of saline vehicle. This expansion in map area was also apparent in the hindlimb motor representation (134 ± 77%, $p = 0.02$, $n = 9$, paired t test), but the expansion was most pronounced in M_{ad} (Figure 6C). The region of overlap between abduction and adduction representations increased in the presence of glutamate receptor antagonists, but was not significantly altered by application of saline (Figure 6D). Because of its influence on map area (Figures S5A and S5B), stimulus intensity was held constant within animals for all pharmacology experiments.

Despite the fact that glutamate receptor antagonists caused map expansion and increased overlap between M_{ab} and M_{ad}, movement topography was not abolished. The M_{ab} and M_{ad} maps could still be distinguished in the presence of glutamate receptor antagonists (Figure 6B), with no significant reduction in the separation between their centers of gravity (Figure 6D). Application of glutamate receptor antagonists did not cause a significantly greater shift in map centers from their baseline positions than application of saline for M_{ab} (0.5 ± 0.09 versus 0.5 ± 0.1 mm, respectively, $p = 0.96$, $n = 9$ versus $n = 5$, t test) or M_{ad} (0.5 ± 0.09 versus 0.2 ± 0.04 mm, respectively, $p = 0.06$).

Although the increased movement durations (Figure 5C) and expansion of motor maps (Figure 6C) caused by disruption of excitatory synaptic transmission were unexpected, this may be explained by a loss of disynaptic inhibition (Helmstaedter et al., 2009; Murayama et al., 2009; Adesnik and Scanziani, 2010; Silberberg and Markram, 2007; Kapfer et al., 2007). To test this hypothesis, we repeated these experiments with

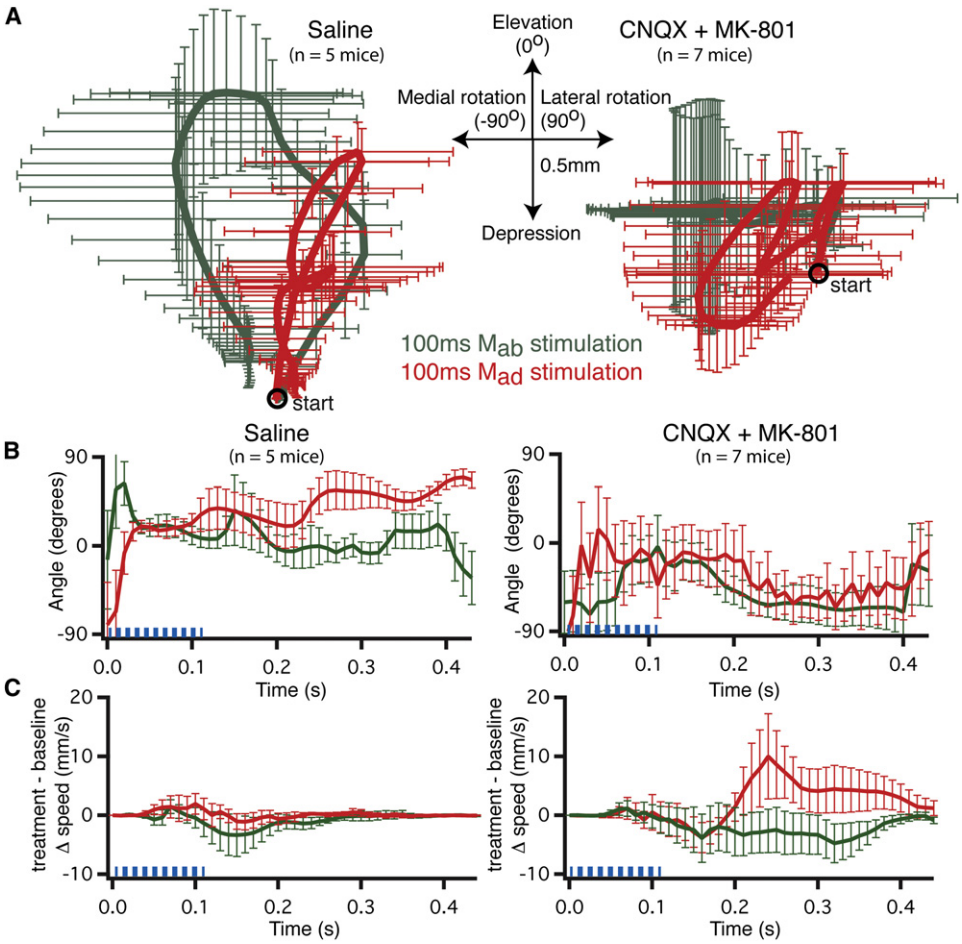

Figure 5. Glutamate Receptor Antagonists Degrade the Differences between Complex Movements Evoked by Prolonged Stimulation of M_{ab} and M_{ad}

(A) Mean trajectories of movements evoked by stimulation (100 ms train of 5 ms pulses at 100 Hz) of M_{ab} (green traces) and M_{ad} (red traces) after application of CNQX and MK-801 (4.5 and 0.3 mM, respectively, right) or saline (left) to the surface of the sensorimotor cortex.

(B) Plots of angle from the start point for the movement trajectories shown in (A) (see compass in (A). Saline-treated control animals (left) displayed movement trajectories that were dependent on stimulus site ($F_{interaction}$ (1,44) = 3.59, $p < 0.001$). Glutamate receptor antagonists degraded the differences between M_{ab} and M_{ad} movements and biased both toward medial rotation (right) $F_{interaction}$ (1,44) = 0.47 p = 0.9984 (see also Figure S6). Dashed blue lines above the abscissae denote the period of stimulation.

(C) Plots of change in speed for the posttreatment movements shown in (A) (pretreatment speed profiles subtracted). There was no effect of saline application (left), but glutamate receptor antagonists caused a site-specific increase in delayed movement speed (right, $F_{interaction}$ (1,44) = 2.079, $p < 0.0001$, RM-ANOVA, n = 7). GABA receptor antagonists similarly altered movement trajectories, but not kinematics (see Figure S7).

Error bars in all graphs are SEM.

$GABA_A$ receptor antagonists (gabazine 1 μM n = 4 or picrotoxin 100 μM n = 2, Figure S6). GABA receptor antagonists diminished differences between M_{ab} and M_{ad} movement trajectories, but had no significant effect on movement kinematics (Figure S6), and generally did not degrade functional subdivisions of the motor cortex. Disrupting GABAergic transmission did reproduce the increases in map amplitude (Figure S7C) and area (Figure S7D) seen during blockade of excitatory transmission. As with the delayed increase in movement speeds (Figure 5C), this effect was restricted to $M_{ad.}$ These effects are consistent with disinhibition causing the selective expansion of the M_{ad} subregion. The separation between M_{ab} and M_{ad} and the region of overlap between them was unchanged (Figure S7E). Like glutamate receptor antagonists, GABA receptor antagonists did not cause greater displacement of map centers than saline treatment for M_{ab} (0.6 ± 0.1 versus 0.5 ± 0.1 mm, p = 0.37, n = 6 versus n = 5, t test) or M_{ad} (0.4 ± 0.1 versus 0.2 ± 0.04 mm, p = 0.24).

Topical Application of Glutamate Receptor Antagonists Disrupts Cortical Input without Preventing Direct Activation of ChR2-Expressing Output Neurons

The observation that disrupting intracortical synaptic transmission can impair the expression of diverse complex movements without abolishing the topography of movement maps was initially surprising, but may be explained by differences between

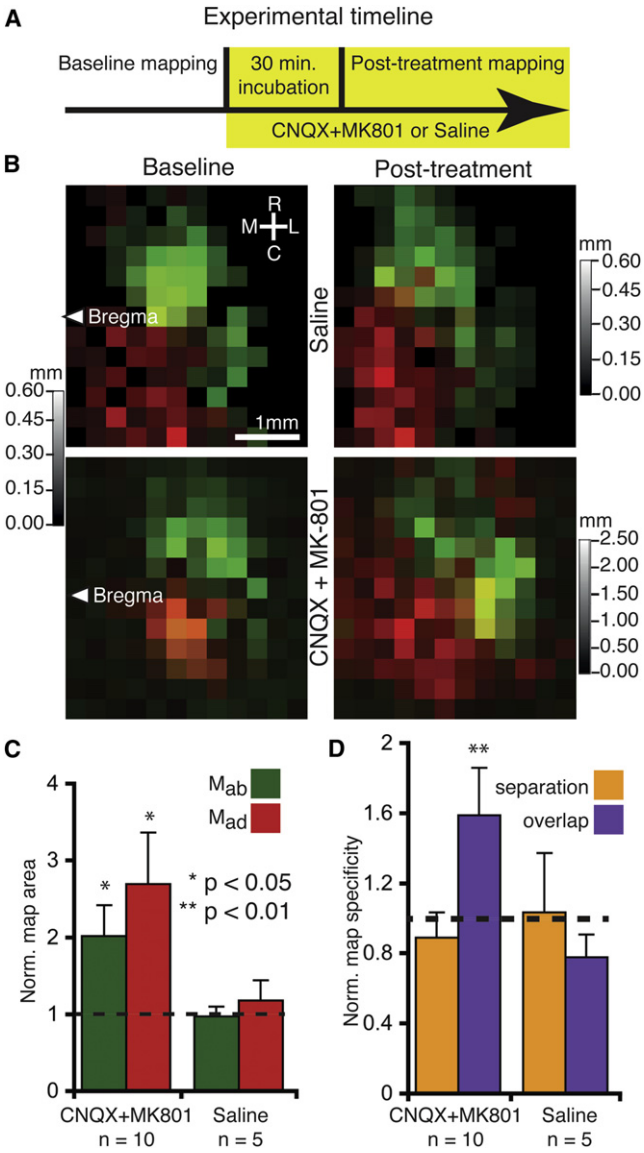

Figure 6. Glutamate Receptor Antagonists Cause Map Expansion without Abolishing Movement Representations

(A) Timeline for pharmacology experiments. Baseline maps were generated before applying either CNQX and MK801 or saline to the cranial window. Posttreatment mapping began after a 30 min incubation period.

(B) Representative movement maps from two different animals before (left) and after (right) pharmacological treatment. Compared with application of saline (top), incubating the cortex with CNQX and MK-801 (4.5 and 0.3 mM, respectively, middle) caused an enlargement both the M_{ab} and M_{ad} representations relative to baseline, but did not cause them to merge (see also Figures S6 and S7). Scale bar at left applies to both maps.

(C) Quantification of increases in map area after application of glutamate receptor antagonists or saline *$p < 0.05$, **$p < 0.01$, paired t test against baseline values). The number of animals per condition is marked for each group.

(D) The region of overlap between M_{ab} and M_{ad} (yellow pixels in map) increased in the presence of glutamate, but separation between the centers of M_{ab} and M_{ad} was unchanged.

Error bars in all graphs are SEM.

the roles of intracortical and corticofugal circuits. It is possible that cortical application of receptor antagonists interferes with local circuit function and the generation of complex movements by prolonged stimulation, but does not alter the movement maps generated by the output of corticofugal cells directly activated by brief pulses of optogenetic excitation. To measure the effect of glutamate receptor antagonists on cortical activity evoked by ChR2 stimulation, we recorded local field potentials (LFPs) in all cortical layers using a multichannel probe (Figure 7). These recordings confirmed that glutamate receptor antagonists blocked synaptic input to the cortex driven by electrical stimulation of the contralateral forelimb. Glutamate receptor antagonists did not block direct activation of ChR2, but they did cause a decrease in delayed, presumably synaptic, components (Figure 7A). This effect was evident at all depths recorded (Figure 7B), but may have been primarily due to inactivation of the upper cortical layers, where drug concentrations are expected to be highest after topical application. Because optogenetic stimulation of ChR2-expressing neurons does not require synaptic activation, corticofugal neurons could still propagate their action potentials beyond the influence of the cortically applied glutamate receptor antagonists to evoke movements.

Divergent Projections from M_{ab} and M_{ad}

The fact that cortical application of glutamate receptor antagonists does not abolish movement topography (Figure 6) or prevent direct activation of corticofugal ChR2-expressing neurons (Figure 7) suggests that cortical output circuits may differentiate the M_{ab} and M_{ad} subregions. To test this hypothesis, we injected the deep cortical layers of M_{ab} and M_{ad} with adeno-associated virus containing fluorescent marker constructs to label axonal projections throughout the brain (Figure 8A). In addition to reciprocal intracortical projections between these regions and trans-callosal projections to homotopic sensorimotor cortex, we observed adjacent, nonoverlapping projections in the striatum and internal capsule (Figures 8B and 8C), with fibers originating in M_{ab} occupying positions medial to those from M_{ad} (2.0 ± 0.1 versus 2.5 ± 0.07 mm from midline in the dorsolateral striatum, $p = 0.03$, $n = 7$, paired t test; Figure 8D). This observation further supports the hypothesis that movement map topography is a product of the pattern of corticofugal projections, whereas the generation of complex movements by prolonged stimulation requires input from recurrent intracortical circuits and/or loops with subcortical structures.

DISCUSSION

We have applied light-based motor mapping to reveal that the mouse forelimb motor cortex is subdivided into distinct movement representations. Prolonged stimulation of these regions drives movements with similar speed profiles, but which terminate at different positions in space. Although complex movements evoked by prolonged stimulation were sensitive to perturbations of intracortical synaptic transmission, the topography of movement direction was not abolished by blockade of either excitatory or inhibitory synaptic transmission. The persistence of movement topography in spite of disrupted intracortical synaptic transmission may be due to the presence of

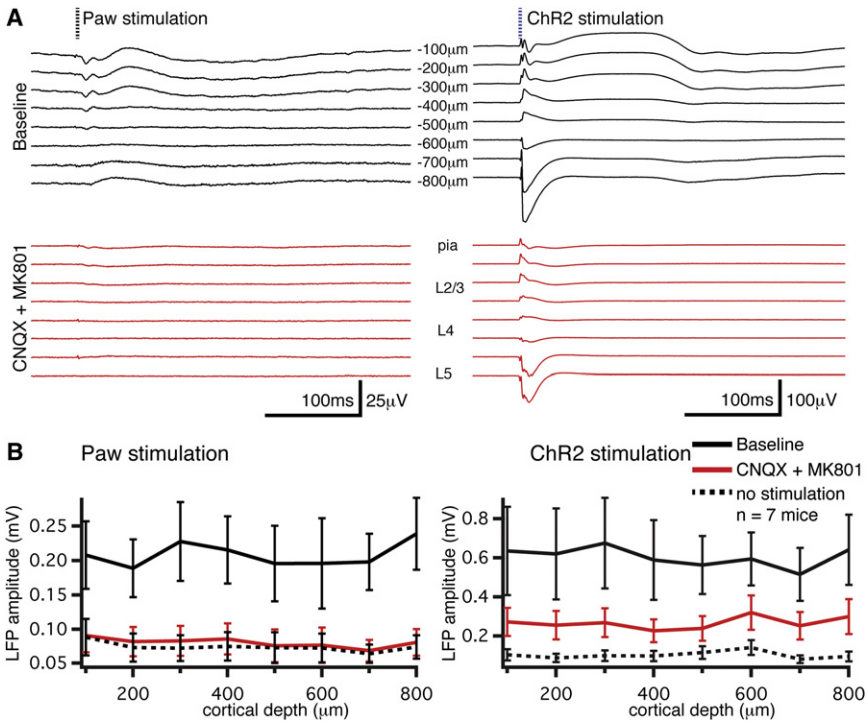

Figure 7. Glutamate Receptor Antagonists Block Cortical Synaptic Transmission but Not Direct Activation of ChR2-Positive Neurons

(A) Representative local field potentials (LFPs, mean of 50 trials) evoked by electrical stimulation of the contralateral paw (left, stimulus time marked with dashed line) or by cortical stimulation with blue light (right). After application of CNQX and MK-801 (bottom), activity evoked by paw stimulation, but not ChR2 stimulation, was blocked.

(B) Mean LFP amplitudes recorded before (baseline, solid black lines) and after (CNQX+MK801, red lines) application of glutamate receptor antagonists. The peak-to-peak amplitude was measured in a time window 300 ms after paw stimulation (left) or ChR2 stimulation (right). After application of CNQX and MK801, LFP deflections evoked by paw stimulation were not greater than spontaneous fluctuations recorded in the absence of stimulation (control, dashed black line; $F(1,7) = 3.76$, $p = 0.06$, RM-ANOVA, n = 7 mice). Conversely, ChR2-evoked LFP amplitudes were still present after application of CNQX and MK801 ($F(1,7) = 25.78$, $p < 0.0001$). Application of CNQX+MK801 caused a significant reduction in LFP amplitudes evoked by both paw ($F[1,7] = 114.9$, $p < 0.0001$) and ChR2 stimulation ($F[1,7] = 18.29$, $p < 0.0001$, RM-ANOVA, n = 7 mice). Error bars in all graphs are SEM.

segregated corticofugal pathways from the two movement representations.

Mechanistic Basis of Multiple Motor Representations

Functional differences between movement representations are likely the product of both their intracortical circuits (Jacobs and Donoghue, 1991; Rouiller et al., 1993) and their corticofugal pathways (Brown and Hestrin, 2009; Rathelot and Strick, 2009). The recurrent circuitry of the neocortex (Douglas and Martin, 2004; Hooks et al., 2011) provides computational power and allows flexible control of the more stereotyped connections between the spinal cord and the periphery. We have shown that the ability of prolonged cortical stimulation to generate complex movement patterns depends upon these intracortical circuits, and can be blocked by pharmacological manipulations. The contribution of recurrent cortical circuitry to movement representations is evidenced by their rapid modification in response to pharmacological manipulations (Jacobs and Donoghue, 1991) or inhibition of protein synthesis (Kleim et al., 2003) and their rewiring after injury (Dancause et al., 2005). Expansion of representations after application of both glutamate and GABA receptor antagonists is presumably due to a loss of disynaptic inhibition, consistent with previous work (Jacobs and Donoghue, 1991; Aroniadou and Keller, 1993; Hess and Donoghue, 1994; Schneider et al., 2002; Foeller et al., 2005). The critical role of inhibitory circuits in cortical function and the profound change in brain state induced by application of GABA receptor antagonists complicates interpretation of our GABA experiments, but it is interesting to note that the effects of this manipulation were relatively specific to the M_{ad} representation (Figure S7).

Our observation that distinct cortical movement representations persisted after the pharmacological disruption of intracortical synaptic transmission suggests that the corticofugal projections made by these regions play a key role in shaping movement representations, as has been reported for the whisker motor pathway of mice (Matyas et al., 2010) and monkey motor cortex (Rathelot and Strick, 2009). Light-based motor mapping using line 18 *Thy-1* transgenic mice (Ayling et al., 2009; Hira et al., 2009; Komiyama et al., 2010) is particularly well suited to defining the contribution of corticofugal projections to motor topography since layer 5b pyramidal neurons are preferentially labeled (Yu et al., 2008; Ayling et al., 2009).

The macroscopic parcellation of motor cortex into functionally distinct zones is particularly intriguing given that neuronal response types appear to be intermingled at the cellular level in rodents (Ohki et al., 2005; Dombeck et al., 2009; Komiyama et al., 2010; Wang et al., 2011). This apparent paradox may be resolved if movement representations are emergent phenomena that only materialize at the population level (Georgopoulos et al., 1986; Wessberg et al., 2000). Alternatively, this observation could reflect important differences between the layer 2/3 cortical neurons studied in many imaging experiments and the predominantly layer 5b neurons stimulated in light-based mapping.

Movement Representations in Rodents and Primates

Multiple motor representations of the rodent forelimb have previously been described as the caudal and rostral forelimb areas (CFA and RFA) (Neafsey and Sievert, 1982). Although M_{ab} and M_{ad} occupy the same cortical territory as mouse CFA and RFA (Tennant et al., 2011), important differences exist between

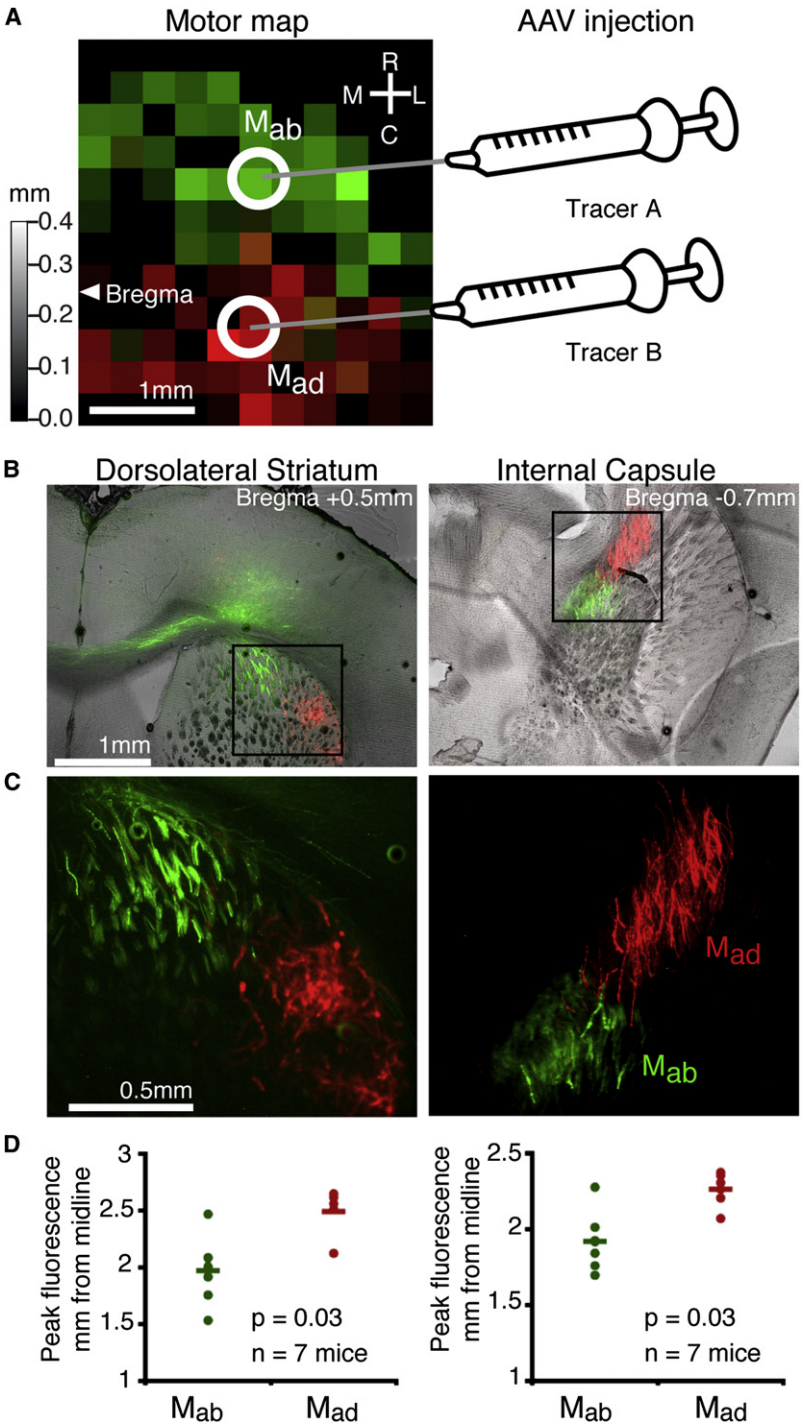

Figure 8. M_{ab} and M_{ad} Have Adjacent, Nonoverlapping Corticofugal Projection Pathways

(A) Representative motor map generated through a thinned-skull preparation (left) to target the centers of gravity of M_{ab} and M_{ad} with injections of anterograde viral tracers (right).

(B) Fibers from M_{ab} (green) and M_{ad} (red) in the dorsolateral striatum (left) and internal capsule (right) in another representative animal.

(C) Magnified details of the inset sections above demonstrating that projections from M_{ab} and M_{ad} had little overlap.

(D) Average distance from midline of peak fluorescence intensity for projections from M_{ab} (green) and M_{ad} (red) in the dorsolateral striatum (left, 1.97 + 0.11 mm versus 2.49 + 0.07 mm, $p = 0.03$, t test, $n = 7$ mice) and internal capsule (right, 1.92 + 0.07 mm versus 2.26 + 0.02 mm, $p = 0.03$, t test, $n = 7$ mice). Note that images were rotated until the midline was vertical before quantification.

Error bars in all graphs are SEM.

them. First, M_{ab} and M_{ad} are contiguous and equal in area, whereas CFA is larger than RFA and they are separated by a representation of the neck (Tennant et al., 2011). Second, RFA is not apparent in all experiments or animals (Tennant et al., 2011), whereas M_{ab} and M_{ad} almost always co-occur. It is interesting to note that in rats, mapping with short stimulus durations produces maps that include RFA and CFA, whereas long (500 ms) durations reveal maps containing movement representations similar to M_{ab} and M_{ad} (Ramanathan et al., 2006).

Primate motor cortex is commonly described as a hierarchical arrangement of primary motor cortex, premotor areas, and supplementary motor cortex where premotor areas can facilitate motor output from primary motor cortex (Cerri et al., 2003). It has been suggested based on their connectivity that rodent RFA and CFA are homologous to premotor and primary motor cortex, respectively (Rouiller et al., 1993). Our observation that M_{ad} expands after application of GABA receptor antagonists but M_{ab} does not suggests that these regions may be differentially regulated by feed-forward or lateral inhibition. Coupled with the relatively longer latencies for movements evoked from the more caudal M_{ad} region, this could be viewed as evidence for a hierarchical arrangement of mouse motor cortex.

Although intracortical connections are obviously critical for motor function, it is also known that multiple motor cortical regions project in parallel to the spinal cord (Rouiller et al., 1993; Dum and Strick, 2002). This implies that multiple motor regions can contribute directly to movement, and may not be arranged hierarchically (Graziano and Aflalo, 2007). This view is corroborated by the results of our experiments with glutamate and GABA receptor antagonists, which demonstrated that the M_{ab} and M_{ad} representations could function independently after a diminution of intracortical synaptic transmission. If multiple motor regions do not form a hierarchical chain, they may instead encode various behaviors or postures (Graziano et al., 2002, 2005). This is consistent with our observation that stimulation of M_{ab} and M_{ad} drives limb movements to different

end positions in space. This result could be produced with optogenetic or electrical stimulation, suggesting that it is not an artifact of passive electrical current spread from the stimulation site (Strick, 2002). Although we sometimes observed movements that resembled locomotion (combined rhythmic movements of contralateral forelimb and hindlimb upon stimulation of M_{ad}), or manipulation (stimulation of M_{ab} generally caused elevation and medial rotation to bring the contralateral forelimb to a central position in front of the body, Movie S2), we chose to focus our analysis on basic measures of motor behavior, such as movement direction.

Comparison of Optogenetic and Electrical Motor Mapping

Our light-based motor mapping technique has been optimized for speed and simplicity (Ayling et al., 2009); hence, measurements of limb movement were made in a single dimension during mapping, or in two dimensions for video analysis. ICMS has been optimized to resolve select movements of single joints (Burish et al., 2008; Chakrabarty et al., 2009; Young et al., 2011), something that is not observed with our technique in its present form. As a consequence, we are overlooking some of the complexity of evoked movements during mapping, and it is likely that the mouse motor cortex could be subdivided more finely based on a more advanced quantitative assay. These disadvantages of light-based mapping are offset by its unique ability to rapidly, objectively, and noninvasively quantify motor output of a defined cell type across the entire sensorimotor cortex.

The spatial resolution of light-based mapping is determined by physical scattering of light and by active spread of excitation. The influence of these factors is apparent from the observation that motor map area is strongly related to both stimulus intensity (Figure S5) and anesthetic depth (Tandon et al., 2008). A further limit on spatial resolution could be imposed by the width of ChR2-expressing pyramidal neurons' overlapping dendritic arbors. Although the lateral resolution of light-based mapping may limit our ability to define exact boundaries of motor representations, we are able to resolve functional subregions of the forelimb motor cortex and generate maps of the hindlimb motor cortex that are often less than a millimeter in diameter (Ayling et al., 2009). Furthermore, blocking the synaptic spread of activation does not decrease the size of motor maps, suggesting that active spread of excitation does not substantially degrade map resolution (Figure 6). It is interesting to note that although motor map area decreases with reduced stimulus intensity, distinct M_{ab} and M_{ad} representations persist and separation between them actually increases (Figure S5). Furthermore, the cortical area activated by optogenetic stimulation is estimated to be only modestly larger than for electrical stimulation based on intrinsic signal imaging (Ayling et al., 2009). This difference may be offset by the selective expression of ChR2 in corticofugal output neurons, which could avoid stimulating axons of passage. Light-based mapping also benefits from advantages in sampling, since stimulation sites can be distributed uniformly, spaced densely, and sampled repeatedly to accurately define the center of a motor map. Despite the biophysical differences between optogenetic and electrical stimulation, light-based maps generally resemble motor maps produced by electrical stimulation (Ramanathan et al., 2006; Tennant et al., 2011). Movement trajectories characteristic of M_{ab} or M_{ad} could be evoked using electrical or optogenetic stimulation, suggesting that similar neuronal populations are recruited by these methods. This finding supports the ability of ICMS to selectively target restricted ensembles of cortical neurons.

A Rodent Model of Motor Circuitry for Complex Movements

The ability to reproducibly evoke distinct complex movements from multiple cortical sites presents an opportunity to perform further investigations of motor circuitry in a widely used model organism. More importantly, it will allow the advantages of genetic engineering in mice to be applied to the problem of motor cortex function and organization, either for optical circuit analysis (Zhang et al., 2007; Tian et al., 2009; Chow et al., 2010) or in the search for future treatments for movement disorders, cortical injuries, and paralysis (Hodgson et al., 1999; Dancause, 2006; Murphy and Corbett, 2009; Dawson et al., 2010; Vargas-Irwin et al., 2010).

EXPERIMENTAL PROCEDURES

Animals and Surgery

Animal protocols were approved by the University of British Columbia Animal Care Committee. Channelrhodopsin-2 transgenic mice (Arenkiel et al., 2007) from Jackson Labs (line 18, stock 007612, strain B6.Cg-Tg(Thy1-COP4/EYFP)18Gfng/J) established a breeding colony. Adult mice aged 2–6 months and weighing 20–30 g were used for these experiments. Isoflurane anesthesia was used during surgery and intrinsic optical signal imaging of somatosensory representations, but was replaced by ketamine/xylazine (100/10 mg/kg, supplemented at 1/10th initial dose as necessary) prior to motor mapping. Craniectomies were performed on transgenic mice used in acute experiments, but virally transduced mice (see section below for details on injections) were mapped through the intact skull due to concern that multiple cranial surgeries could damage the cortex. Chronic mapping was performed through a cranial window (Harrison et al., 2009).

Light-Based Motor Mapping

Light-based mapping methodology has been described in detail (Ayling et al., 2009). Briefly, we used a scanning stage (ASI MS-2000) controlled by custom Igor Pro software (Wavemetrics) to direct a fixed 473 nm laser beam (Crystalaser, focused to 100 μm diameter, 10 ms pulses, 0.5–10 mW total or 63–1,270 mW/mm^2) to an array of cortical sites (typically 13 × 13, with 300 μm spacing between sites). This process was repeated three to five times to obtain a mean value for each pixel of the map. Stimulation was delivered in a semi-random order with identical stimulus intensity for all sites within a map. Movements were detected using laser range finders with mm sensitivity targeted to the forelimb and hindlimb (Keyence LK-081). In order to exclude artifacts (e.g., from breathing or electrical noise), responses were considered to be genuine only if their amplitude exceeded three times the standard deviation of the 500 ms prestimulus period within 100 ms after stimulus onset.

Map Analysis

Motor maps were generated by plotting the peak amplitude of the mean movement profile corresponding to each cortical site of stimulation. Amplitude was quantified within a 300 ms time window after laser stimulation. If the amplitude of the movement evoked at that site was positive, the corresponding pixel was added to the adduction map. If the amplitude had a negative value with respect to the baseline, that site was added to the abduction map. In the case of bidirectional movement profiles where both the positive and negative components

satisfied the amplitude criteria, the corresponding site was included in both the abduction and adduction maps and counted as overlap between maps. For each map, the center of gravity was calculated along with the mean amplitude and latency for the nine pixels closest to the center point. Maps with mean amplitude of <0.1 mm at the center were excluded from further analysis. Separation between M_{ab} and M_{ad} was defined as the distance between the centers of gravity for each map.

Video Capture of Evoked Movements in Anesthetized Mice

After completing two to five motor maps, mice were raised into a sitting posture with their forelimbs hanging freely. Stimulus sites were placed as close to the centers of the abduction and adduction representations as possible without targeting major blood vessels, since these absorb light strongly (Ayling et al., 2009). Fifty-one frames were captured at a rate of 100 Hz beginning 10 ms prior to laser stimulus onset, and paw trajectories were generated from the raw image sequences using the plugin "MTrack2" for ImageJ. Ten to 20 repetitions were then averaged for each trial, and speed and angle profiles were calculated based on this average trajectory.

Video Capture of Evoked Movements in Awake Mice

ChR2 transgenic mice were implanted with optical fibers (Thorlabs BFH48-200) extending to the cortical surface and terminating in a ferrule connector (Precision Fiber Products) fixed to the skull with dental acrylic and bone screws. Two fibers were implanted, targeted to the mean coordinates of the M_{ab} and M_{ad} map centers. These locations were stimulated alternately (5 mW 5 ms pulses at 100 Hz for 500 ms) using a 473 nm laser (IKECOOL IKE-473-100-OP) connected via an optical commutator (Doric). Stimulus evoked behavior was recorded by a CCD camera (Dalsa 1M60) and frame grabber (EPIX). Limb trajectories were analyzed in the same manner as the anesthetized data, except that paw position was tracked using the plugin "Manual Tracking" for ImageJ.

Intracortical Microstimulation

Glass pipets (tip width 10–20 μm) containing a 0.25 mm bare silver wire were filled with 1% fast green in 3 M sodium chloride. A micromanipulator (Sutter) was used to advance the pipet to a depth of 700 μm. Stimulation sites were matched with those targeted by laser stimulation in the same animals. Trains of 200 μs 100 μA pulses at 200 Hz with 10–500 ms durations were generated by an AM systems stimulator and a WPI stimulus isolator.

Virus Injections and Anatomical Tracing

For motor mapping experiments involving virally transduced mice, 1–2 μl of adeno-associated virus (serotype 2/1 CAG-ChR2-GFP) was injected through a burr hole into the sensorimotor cortex of ChR2-negative mice 2 mm lateral of bregma at a depth of 500 μm using a 5 μl Hamilton syringe with a 33 gauge needle and a syringe pump (WPI). Mice recovered for 2–4 weeks before being used in experiments. For anatomical tracing experiments, M_{ab} and M_{ad} were identified by light-based mapping through the intact skull of ChR2 transgenic mice (Hira et al., 2009). Injections were made using a custom pressure injection system (Cetin et al., 2006). At each site, 250 nl of virus (turboRFP, mCerulean, or eGFP, with matched serotypes 2/1 or 2/9) was injected over 10 min at a depth of 500 μm. Fluorophore placement in M_{ab} versus M_{ad} was alternated between animals. In three of seven animals, motor maps could not be produced by transcranial stimulation, and injections were targeted to the mean coordinates of M_{ab} and M_{ad}. Three weeks after injection, the mice were transcardially perfused and 100 μm coronal sections were sliced on a vibratome, with every third section mounted for epifluorescence imaging. Fluorescence plots from midline were smoothed and averaged, and the mean position of peak fluorescence was calculated for each animal.

Pharmacology

For experiments involving glutamate receptor antagonists, CNQX (4.5 mM) and MK801 (300 μM), gabazine (1 μM), or picrotoxin (100 μM) in physiological saline solution were applied to the craniectomy. The compounds were allowed to incubate for 30 min before mapping resumed, and were replenished (at the same concentration) every ~30 min throughout the experiment. Control experiments were identical except that saline solution was applied in place of the drugs.

Local Field Potential Recordings

A NeuroNexus multi-site electrode (A1-X16-3mm-50-413) was lowered 800 μm into sensorimotor cortex using a micromanipulator (Sutter), and a reference electrode was immersed in the saline bathing the cortical surface. In each experiment, at least 50 trials of 1 ms, 0.1 Hz electrical (1 mA), and ChR2 (10 mW 473 nm) stimulation were recorded, and then CNQX and MK801 were applied to the cortical surface as above and incubated for 30 min before recordings were repeated. The mean peak-to-peak amplitude was measured in a time window of 300 ms after stimulus onset for each electrode contact. The mean amplitude of the baseline noise was subtracted, and adjacent electrode contacts were binned by averaging.

SUPPLEMENTAL INFORMATION

Supplemental Information includes seven figures, Supplemental Experimental Procedures, and two movies and can be found with this article online at doi:10.1016/j.neuron.2012.02.028.

ACKNOWLEDGMENTS

This work was supported by a Canadian Institutes of Health Research (CIHR) Operating Grant MOP-12675, a Human Frontier Science Program grant, and funding from the estate of Erika W. White to T.H.M. T.C.H. holds a CIHR Vanier scholarship and a Michael Smith Foundation for Health Research (MSFHR) graduate scholarship and held a National Sciences and Engineering Research Council (NSERC) scholarship and a University of British Columbia College for Interdisciplinary Studies scholarship. O.G.S.A. held a CIHR graduate studentship. We would like to acknowledge the assistance of Cindy Jiang for animal husbandry and surgery, Jamie Boyd for programming, Jeff Ledue for optical design, Shangbin Chen and Nadia Scott for in vivo electrophysiology, and Michael Baratta and Ed Boyden for optical fiber assembly techniques and advice. We thank Karl Deisseroth for the AAV-ChR2 obtained from the University of Pennsylvania vector core.

Accepted: February 9, 2012
Published: April 25, 2012

REFERENCES

Adesnik, H., and Scanziani, M. (2010). Lateral competition for cortical space by layer-specific horizontal circuits. Nature *464*, 1155–1160.

Anderson, C.T., Sheets, P.L., Kiritani, T., and Shepherd, G.M.G. (2010). Sublayer-specific microcircuits of corticospinal and corticostriatal neurons in motor cortex. Nat. Neurosci. *13*, 739–744.

Arenkiel, B.R., Peca, J., Davison, I.G., Feliciano, C., Deisseroth, K., Augustine, G.J., Ehlers, M.D., and Feng, G. (2007). In vivo light-induced activation of neural circuitry in transgenic mice expressing channelrhodopsin-2. Neuron *54*, 205–218.

Aroniadou, V.A., and Keller, A. (1993). The patterns and synaptic properties of horizontal intracortical connections in the rat motor cortex. J. Neurophysiol. *70*, 1553–1569.

Asanuma, H., and Rosén, I. (1972). Topographical organization of cortical efferent zones projecting to distal forelimb muscles in the monkey. Exp. Brain Res. *14*, 243–256.

Ayling, O.G.S., Harrison, T.C., Boyd, J.D., Goroshkov, A., and Murphy, T.H. (2009). Automated light-based mapping of motor cortex by photoactivation of channelrhodopsin-2 transgenic mice. Nat. Methods *6*, 219–224.

Brown, S.P., and Hestrin, S. (2009). Intracortical circuits of pyramidal neurons reflect their long-range axonal targets. Nature *457*, 1133–1136.

Burish, M.J., Stepniewska, I., and Kaas, J.H. (2008). Microstimulation and architectonics of frontoparietal cortex in common marmosets (Callithrix jacchus). J. Comp. Neurol. *507*, 1151–1168.

Cerri, G., Shimazu, H., Maier, M.A., and Lemon, R.N. (2003). Facilitation from ventral premotor cortex of primary motor cortex outputs to macaque hand muscles. J. Neurophysiol. *90*, 832–842.

Cetin, A., Komai, S., Eliava, M., Seeburg, P.H., and Osten, P. (2006). Stereotaxic gene delivery in the rodent brain. Nat. Protoc. *1*, 3166–3173.

Chakrabarty, S., Friel, K.M., and Martin, J.H. (2009). Activity-dependent plasticity improves M1 motor representation and corticospinal tract connectivity. J. Neurophysiol. *101*, 1283–1293.

Chow, B.Y., Han, X., Dobry, A.S., Qian, X., Chuong, A.S., Li, M., Henninger, M.A., Belfort, G.M., Lin, Y., Monahan, P.E., and Boyden, E.S. (2010). High-performance genetically targetable optical neural silencing by light-driven proton pumps. Nature *463*, 98–102.

Churchland, M.M., Santhanam, G., and Shenoy, K.V. (2006). Preparatory activity in premotor and motor cortex reflects the speed of the upcoming reach. J. Neurophysiol. *96*, 3130–3146.

Dancause, N. (2006). Vicarious function of remote cortex following stroke: recent evidence from human and animal studies. Neuroscientist *12*, 489–499.

Dancause, N., Barbay, S., Frost, S.B., Plautz, E.J., Chen, D., Zoubina, E.V., Stowe, A.M., and Nudo, R.J. (2005). Extensive cortical rewiring after brain injury. J. Neurosci. *25*, 10167–10179.

Dawson, T.M., Ko, H.S., and Dawson, V.L. (2010). Genetic animal models of Parkinson's disease. Neuron *66*, 646–661.

Dombeck, D.A., Graziano, M.S., and Tank, D.W. (2009). Functional clustering of neurons in motor cortex determined by cellular resolution imaging in awake behaving mice. J. Neurosci. *29*, 13751–13760.

Douglas, R.J., and Martin, K.A.C. (2004). Neuronal circuits of the neocortex. Annu. Rev. Neurosci. *27*, 419–451.

Dum, R.P., and Strick, P.L. (2002). Motor areas in the frontal lobe of the primate. Physiol. Behav. *77*, 677–682.

Evarts, E.V. (1968). Relation of pyramidal tract activity to force exerted during voluntary movement. J. Neurophysiol. *31*, 14–27.

Flaherty, A.W., and Graybiel, A.M. (1991). Corticostriatal transformations in the primate somatosensory system. Projections from physiologically mapped body-part representations. J. Neurophysiol. *66*, 1249–1263.

Foeller, E., Celikel, T., and Feldman, D.E. (2005). Inhibitory sharpening of receptive fields contributes to whisker map plasticity in rat somatosensory cortex. J. Neurophysiol. *94*, 4387–4400.

Fritsch, G., and Hitzig, E. (1870). Electric excitability of the cerebrum (Uber die elektrische Erregbarkeit des Grosshirns). Epilepsy Behav. *15*, 123–130.

Gallese, V., Fadiga, L., Fogassi, L., and Rizzolatti, G. (1996). Action recognition in the premotor cortex. Brain *119*, 593–609.

Georgopoulos, A.P., Schwartz, A.B., and Kettner, R.E. (1986). Neuronal population coding of movement direction. Science *233*, 1416–1419.

Graziano, M.S.A., and Aflalo, T.N. (2007). Rethinking cortical organization: moving away from discrete areas arranged in hierarchies. Neuroscientist *13*, 138–147.

Graziano, M.S.A., Taylor, C.S.R., and Moore, T. (2002). Complex movements evoked by microstimulation of precentral cortex. Neuron *34*, 841–851.

Graziano, M.S.A., Aflalo, T.N.S., and Cooke, D.F. (2005). Arm movements evoked by electrical stimulation in the motor cortex of monkeys. J. Neurophysiol. *94*, 4209–4223.

Hari, R., Forss, N., Avikainen, S., Kirveskari, E., Salenius, S., and Rizzolatti, G. (1998). Activation of human primary motor cortex during action observation: a neuromagnetic study. Proc. Natl. Acad. Sci. USA *95*, 15061–15065.

Harrison, T.C., Sigler, A., and Murphy, T.H. (2009). Simple and cost-effective hardware and software for functional brain mapping using intrinsic optical signal imaging. J. Neurosci. Methods *182*, 211–218.

Helmstaedter, M., Sakmann, B., and Feldmeyer, D. (2009). Neuronal correlates of local, lateral, and translaminar inhibition with reference to cortical columns. Cereb. Cortex *19*, 926–937.

Hess, G., and Donoghue, J.P. (1994). Long-term potentiation of horizontal connections provides a mechanism to reorganize cortical motor maps. J. Neurophysiol. *71*, 2543–2547.

Hira, R., Honkura, N., Noguchi, J., Maruyama, Y., Augustine, G.J., Kasai, H., and Matsuzaki, M. (2009). Transcranial optogenetic stimulation for functional mapping of the motor cortex. J. Neurosci. Methods *179*, 258–263.

Hodgson, J.G., Agopyan, N., Gutekunst, C.A., Leavitt, B.R., LePiane, F., Singaraja, R., Smith, D.J., Bissada, N., McCutcheon, K., Nasir, J., et al. (1999). A YAC mouse model for Huntington's disease with full-length mutant huntingtin, cytoplasmic toxicity, and selective striatal neurodegeneration. Neuron *23*, 181–192.

Hooks, B.M., Hires, S.A., Zhang, Y.-X., Huber, D., Petreanu, L., Svoboda, K., and Shepherd, G.M.G. (2011). Laminar analysis of excitatory local circuits in vibrissal motor and sensory cortical areas. PLoS Biol. *9*, e1000572.

Hoover, J.E., and Strick, P.L. (1993). Multiple output channels in the basal ganglia. Science *259*, 819–821.

Jacobs, K.M., and Donoghue, J.P. (1991). Reshaping the cortical motor map by unmasking latent intracortical connections. Science *251*, 944–947.

Kapfer, C., Glickfeld, L.L., Atallah, B.V., and Scanziani, M. (2007). Supralinear increase of recurrent inhibition during sparse activity in the somatosensory cortex. Nat. Neurosci. *10*, 743–753.

Kelly, R.M., and Strick, P.L. (2003). Cerebellar loops with motor cortex and prefrontal cortex of a nonhuman primate. J. Neurosci. *23*, 8432–8444.

Kleim, J.A., Bruneau, R., Calder, K., Pocock, D., VandenBerg, P.M., MacDonald, E., Monfils, M.H., Sutherland, R.J., and Nader, K. (2003). Functional organization of adult motor cortex is dependent upon continued protein synthesis. Neuron *40*, 167–176.

Komiyama, T., Sato, T.R., O'Connor, D.H., Zhang, Y.-X., Huber, D., Hooks, B.M., Gabitto, M., and Svoboda, K. (2010). Learning-related fine-scale specificity imaged in motor cortex circuits of behaving mice. Nature *464*, 1182–1186.

Luppino, G., Matelli, M., Camarda, R.M., Gallese, V., and Rizzolatti, G. (1991). Multiple representations of body movements in mesial area 6 and the adjacent cingulate cortex: an intracortical microstimulation study in the macaque monkey. J. Comp. Neurol. *311*, 463–482.

Matyas, F., Sreenivasan, V., Marbach, F., Wacongne, C., Barsy, B., Mateo, C., Aronoff, R., and Petersen, C.C.H. (2010). Motor control by sensory cortex. Science *330*, 1240–1243.

Moran, D.W., and Schwartz, A.B. (1999). Motor cortical representation of speed and direction during reaching. J. Neurophysiol. *82*, 2676–2692.

Murayama, M., Pérez-Garci, E., Nevian, T., Bock, T., Senn, W., and Larkum, M.E. (2009). Dendritic encoding of sensory stimuli controlled by deep cortical interneurons. Nature *457*, 1137–1141.

Murphy, T.H., and Corbett, D. (2009). Plasticity during stroke recovery: from synapse to behaviour. Nat. Rev. Neurosci. *10*, 861–872.

Neafsey, E.J., and Sievert, C. (1982). A second forelimb motor area exists in rat frontal cortex. Brain Res. *232*, 151–156.

Ohki, K., Chung, S., Ch'ng, Y.H., Kara, P., and Reid, R.C. (2005). Functional imaging with cellular resolution reveals precise micro-architecture in visual cortex. Nature *433*, 597–603.

Paz, R., Boraud, T., Natan, C., Bergman, H., and Vaadia, E. (2003). Preparatory activity in motor cortex reflects learning of local visuomotor skills. Nat. Neurosci. *6*, 882–890.

Penfield, W., and Boldrey, E. (1937). Somatic motor and sensory representation in the cerebral cortex of man as studied by electrical stimulation. Brain *60*, 389.

Pronichev, I.V., and Lenkov, D.N. (1998). Functional mapping of the motor cortex of the white mouse by a microstimulation method. Neurosci. Behav. Physiol. *28*, 80–85.

Ramanathan, D., Conner, J.M., and Tuszynski, M.H. (2006). A form of motor cortical plasticity that correlates with recovery of function after brain injury. Proc. Natl. Acad. Sci. USA *103*, 11370–11375.

Rathelot, J.-A., and Strick, P.L. (2009). Subdivisions of primary motor cortex based on cortico-motoneuronal cells. Proc. Natl. Acad. Sci. USA *106*, 918–923.

Rouiller, E.M., Moret, V., and Liang, F. (1993). Comparison of the connectional properties of the two forelimb areas of the rat sensorimotor cortex: support for the presence of a premotor or supplementary motor cortical area. Somatosens. Mot. Res. *10*, 269–289.

Sanes, J.N., and Donoghue, J.P. (1993). Oscillations in local field potentials of the primate motor cortex during voluntary movement. Proc. Natl. Acad. Sci. USA *90*, 4470–4474.

Schieber, M.H. (2001). Constraints on somatotopic organization in the primary motor cortex. J. Neurophysiol. *86*, 2125–2143.

Schneider, C., Devanne, H., Lavoie, B.A., and Capaday, C. (2002). Neural mechanisms involved in the functional linking of motor cortical points. Exp. Brain Res. *146*, 86–94.

Silberberg, G., and Markram, H. (2007). Disynaptic inhibition between neocortical pyramidal cells mediated by Martinotti cells. Neuron *53*, 735–746.

Stepniewska, I., Fang, P.-C., and Kaas, J.H. (2005). Microstimulation reveals specialized subregions for different complex movements in posterior parietal cortex of prosimian galagos. Proc. Natl. Acad. Sci. USA *102*, 4878–4883.

Strick, P.L. (2002). Stimulating research on motor cortex. Nat. Neurosci. *5*, 714–715.

Tandon, S., Kambi, N., and Jain, N. (2008). Overlapping representations of the neck and whiskers in the rat motor cortex revealed by mapping at different anaesthetic depths. Eur. J. Neurosci. *27*, 228–237.

Tennant, K.A., Adkins, D.L., Donlan, N.A., Asay, A.L., Thomas, N., Kleim, J.A., and Jones, T.A. (2011). The organization of the forelimb representation of the C57BL/6 mouse motor cortex as defined by intracortical microstimulation and cytoarchitecture. Cereb. Cortex *21*, 865–876.

Tian, L., Hires, S.A., Mao, T., Huber, D., Chiappe, M.E., Chalasani, S.H., Petreanu, L., Akerboom, J., McKinney, S.A., Schreiter, E.R., et al. (2009). Imaging neural activity in worms, flies and mice with improved GCaMP calcium indicators. Nat. Methods *6*, 875–881.

Vargas-Irwin, C.E., Shakhnarovich, G., Yadollahpour, P., Mislow, J.M.K., Black, M.J., and Donoghue, J.P. (2010). Decoding complete reach and grasp actions from local primary motor cortex populations. J. Neurosci. *30*, 9659–9669.

Wang, H., Peca, J., Matsuzaki, M., Matsuzaki, K., Noguchi, J., Qiu, L., Wang, D., Zhang, F., Boyden, E., Deisseroth, K., et al. (2007). High-speed mapping of synaptic connectivity using photostimulation in Channelrhodopsin-2 transgenic mice. Proc. Natl. Acad. Sci. USA *104*, 8143–8148.

Wang, L., Conner, J.M., Rickert, J., and Tuszynski, M.H. (2011). Structural plasticity within highly specific neuronal populations identifies a unique parcellation of motor learning in the adult brain. Proc. Natl. Acad. Sci. USA *108*, 2545–2550.

Weiler, N., Wood, L., Yu, J., Solla, S.A., and Shepherd, G.M.G. (2008). Top-down laminar organization of the excitatory network in motor cortex. Nat. Neurosci. *11*, 360–366.

Wessberg, J., Stambaugh, C.R., Kralik, J.D., Beck, P.D., Laubach, M., Chapin, J.K., Kim, J., Biggs, S.J., Srinivasan, M.A., and Nicolelis, M.A.L. (2000). Real-time prediction of hand trajectory by ensembles of cortical neurons in primates. Nature *408*, 361–365.

Young, N.A., Vuong, J., Flynn, C., and Teskey, G.C. (2011). Optimal parameters for microstimulation derived forelimb movement thresholds and motor maps in rats and mice. J. Neurosci. Methods *196*, 60–69.

Yu, J., Anderson, C.T., Kiritani, T., Sheets, P.L., Wokosin, D.L., Wood, L., and Shepherd, G.M.G. (2008). Local-circuit phenotypes of layer 5 neurons in motor-frontal cortex of YFP-H mice. Front Neural Circuits *2*, 6.

Zhang, F., Wang, L.-P., Brauner, M., Liewald, J.F., Kay, K., Watzke, N., Wood, P.G., Bamberg, E., Nagel, G., Gottschalk, A., and Deisseroth, K. (2007). Multimodal fast optical interrogation of neural circuitry. Nature *446*, 633–639.